

Folding lattice proteins with quantum annealing

Anders Irbäck,^{1,*} Lucas Knuthson,¹ Sandipan Mohanty,² and Carsten Peterson¹

¹*Computational Biology & Biological Physics,
Department of Astronomy, and Theoretical Physics,
Lund University, Box 43, SE-221 00 Lund, Sweden*

²*Institute for Advanced Simulation, Jülich Supercomputing Centre,
Forschungszentrum Jülich, D-52425 Jülich, Germany*

(Dated: May 13, 2022)

Abstract

Quantum annealing is a promising approach for obtaining good approximate solutions to difficult optimization problems. Folding a protein sequence into its minimum-energy structure represents such a problem. For testing new algorithms and technologies for this task, the minimal lattice-based HP model is well suited, as it represents a considerable challenge despite its simplicity. The HP model has favorable interactions between adjacent, not directly bound hydrophobic residues. Here, we develop a novel spin representation for lattice protein folding tailored for quantum annealing. With a distributed encoding onto the lattice, it differs from earlier attempts to fold lattice proteins on quantum annealers, which were based upon chain growth techniques. As a result, our approach naturally implements self-avoidance, performs very well in terms of solution quality, and has better scaling properties with chain length. Moreover, the encoding is robust to changes in the parameters required to constrain the spin system to chain-like configurations. The results are evaluated against existing exact results for HP chains with up to $N = 30$ beads with 100% hit rate thereby also outperforming classical simulated annealing. The method also allows us to recover the lowest known energy for an $N = 64$ HP chain. These results are obtained by the commonly used hybrid quantum-classical approach. For pure quantum annealing, our method successfully folds an $N = 14$ HP chain. The calculations were performed on a D-Wave Advantage quantum annealer.

* anders.irback@thep.lu.se

I. INTRODUCTION

Quantum computers with their interacting qubits as basic units appear very promising for optimization problems with binary variables such as those present in spin systems. These technologies are being developed along two main tracks: quantum annealers [1] and gate-based systems [2]. In quantum annealing (QA) [3–5], the idea is to encode the solution to a given optimization problem in the ground state of a Hamiltonian and efficiently locate the energy minimum by exploiting quantum fluctuations and tunneling, in analogy with the role played by thermal fluctuations in classical simulated annealing (SA) [6]. Mapping difficult binary optimization problems onto Ising spin glass systems goes back to the eighties in the context of neural networks [7, 8]. For a recent review, see Ref. [9]. In the context of QA, this approach is called quadratic unconstrained binary optimization (QUBO).

Protein folding, going from sequence to structure by minimizing an energy function, represents a difficult optimization problem. Simplified lattice-based models for this problem can often provide qualitatively relevant results, but remain computationally challenging and are therefore ideal testbeds for novel algorithms. A pioneering QUBO formulation of the folding problem for lattice proteins was given by Perdomo and coworkers [10]. They considered the HP model [11], where proteins are represented by linear chains of N hydrophobic (H) or polar (P) beads, residing on a lattice. Their binary variables encoded bead coordinates on the lattice, which led to a relatively large number of required qubits even for short chains but a polynomial rather than exponential scaling with N .

An early attempt to fold a short lattice protein ($N = 6$) by QA was carried out on a D-Wave (D-Wave Systems Inc.) machine [12]. This implementation relied on a growth algorithm, where turns along the chain were mapped onto qubits. This encoding is resource-efficient for very short chains, but scales exponentially with N . Recent work implemented on an IBM gate-based quantum computer used a similar encoding [13], again for a short protein chain ($N = 7$). These growth algorithms offer a compact chain representation, at the cost of making interactions such as self-avoidance difficult to implement. For a recent review of lattice protein folding on quantum computers, see Ref. [14].

In contrast to Refs. [12, 13], here we propose a different type of mapping, in which all sites of the lattice on which the protein lives host qubits. The approach was inspired by recent D-Wave applications for homopolymers [15], and shares some similarities with a

QUBO formulation for lattice heteropolymers [16] which, to our knowledge, has not yet been implemented. The energy E is such that its minimization makes the values of the qubits coalesce to a finite set of active qubits defining the desired folded structure. Importantly from the viewpoint of QA, the entire function E , including a self-avoidance term, is manifestly quadratic, or two-local, in the binary spin variables. This fully distributed dynamical encoding method can be considered as a clustering approach driven by requiring a legal chain on the lattice. It is also somewhat reminiscent of a molecular field theory [17] where the fields reside on a lattice and give rise to structures through their dynamics.

We evaluate the performance of our approach using the two-dimensional HP model [11] as a testbed. In particular, we consider a set of sequences with up to 30 beads, for which the exact solutions are known from exhaustive enumerations of all structures [18, 19]. In addition, we present results obtained for two longer sequences [20] with 48 and 64 beads, respectively, which have been studied by various classical methods.

In what follows, we first briefly describe the HP model and then map the energy minimization problem for HP sequences to a QUBO problem. We then evaluate our encoding using both classical SA and explorations performed on the D-Wave Advantage quantum annealer, with over 5,000 qubits and 15-way qubit connectivity [21].

II. METHODS

A. HP lattice proteins

We consider the minimal lattice-based HP model for protein folding [11], in which the protein is represented by a self-avoiding chain of hydrophobic (H) or polar (P) beads on a lattice. Two beads are said to be in contact if they are nearest neighbors on the lattice but not along the chain. A given chain configuration is assigned an energy defined as $E_{\text{HP}} = -N_{\text{HH}}$, where N_{HH} is the number of HH contacts [11]. With this choice of energy, low-energy configurations tend to exhibit a hydrophobic core of H beads. Despite the simplicity of the model, there are HP sequences with a unique ground state, and therefore a well-defined structure. In particular, on a 2D square lattice, it is known from exhaustive enumerations that about 2% of all HP sequences with ≤ 30 beads have a unique ground state [18, 19].

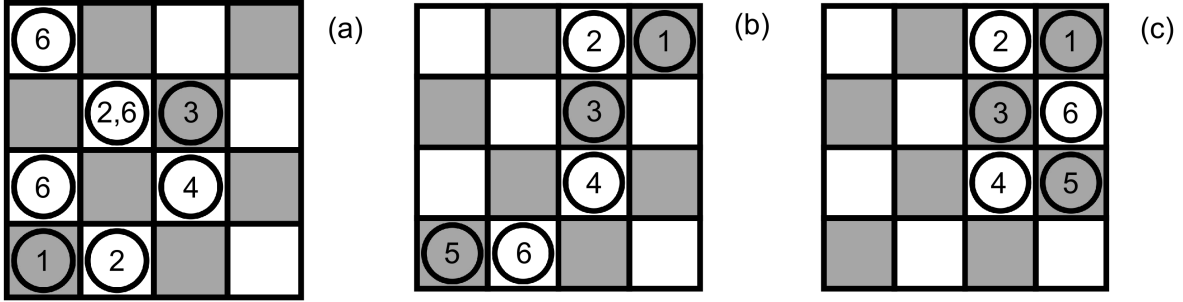


FIG. 1. Illustration of a hypothetical evolution of the binary model described in Sec. II B for the 6-bead sequence HPHPPH. Circles represent beads, and numbers indicate bead positions along the sequence. By construction, odd/even beads can reside only on grey/white sites. (A) Early stage. Typically, all the three constraints are violated ($E_1, E_2, E_3 > 0$). (B) Intermediate stage. Some but not all of the constraints are satisfied (in this example: $E_1 = E_2 = 0, E_3 > 0$). (C) The final state, in this example corresponding to the desired minimum-energy structure of the given sequence ($E_{\text{HP}} = -2, E_1 = E_2 = E_3 = 0$).

B. Binary quadratic model for HP lattice proteins – QUBO encoding

Given an HP sequence (h_1, \dots, h_N) , $h_i \in \{\text{P}, \text{H}\}$, we wish to determine its ground state using QA. To this end, in this section, we present a binary encoding for HP lattice proteins, assuming a square grid with L^2 sites.

Inspired by the binary representation of homopolymers of Ref. [15], rather than directly encoding chain configurations, we introduce fields of binary variables along with penalty terms, the latter of which serve to ensure that the final binary field configurations correspond to proper chain configurations. To reduce the number of binary variables, we make a checkerboard division of the lattice into even and odd sites, and use the fact that in a valid chain configuration all even (odd) beads share the same lattice site parity (see Fig. 1). As a result, we may assume that even (odd) beads reside on even (odd) lattice sites. Thus, we introduce one set of binary fields, σ_s^f , to describe the location of even beads, and another set for odd beads $\sigma_{s'}^{f'}$. Here, the indices f and s run over even beads and sites, respectively, while f' and s' run over odd beads and sites. We set $\sigma_s^f = 1$ if bead f is located on site s , and $\sigma_s^f = 0$ otherwise. The odd fields $\sigma_{s'}^{f'}$ are defined in the same way. The division into even and odd sites reduces the number of variables required from $N \times L^2$ to $\approx N \times L^2/2$.

Having defined the degrees of freedom, we now describe the energy function. In our QUBO model, the total energy E has the form

$$E = E_{\text{HP}} + \sum_{i=1}^3 \lambda_i E_i, \quad (1)$$

where E_{HP} is the energy of the HP model (see above) and the remaining three terms E_1 , E_2 and E_3 are constraint energies. The strengths of the constraints are set by the parameters λ_i .

Specifically, in terms of the binary fields, the four energies can be expressed as follows.

- The HP energy $E_{\text{HP}} = -N_{\text{HH}}$ can be rewritten as

$$E_{\text{HP}} = - \sum_{|f-f'|>1} C(h_f, h_{f'}) \sum_{\langle s, s' \rangle} \sigma_s^f \sigma_{s'}^{f'} \quad (2)$$

where the interaction strength $C(h_f, h_{f'}) = 1$ if $h_f = h_{f'} = \text{H}$ and $C(h_f, h_{f'}) = 0$ otherwise. In Eq. 2, the second sum runs over all nearest-neighbor pairs of sites, $\langle s, s' \rangle$. Such a pair always consist of one even and one odd site. The beads f and f' must both be of type H for a non-zero energy contribution, and must not, with our definition of a contact, be adjacent along the chain.

- The first constraint energy, E_1 , is given by

$$E_1 = \sum_f \left(\sum_s \sigma_s^f - 1 \right)^2 + \{\text{same for odd parity}\}, \quad (3)$$

and serves to ensure that each bead is located at exactly one lattice site.

- The energy E_2 makes the chain self-avoiding. It is given by

$$E_2 = \frac{1}{2} \sum_{f_1 \neq f_2} \sum_s \sigma_s^{f_1} \sigma_s^{f_2} + \{\text{same for odd parity}\}, \quad (4)$$

and provides an energy penalty whenever two beads occupy the same site.

- The final energy, E_3 , has the form

$$E_3 = \sum_{1 \leq f < N} \sum_s \sigma_s^f \sum_{\|s'-s\|>1} \sigma_{s'}^{f+1} + \{\text{same with odd/even parity interchanged}\}, \quad (5)$$

and is responsible for connecting the beads to a chain. It provides an energy penalty whenever two adjacent beads along chain are not nearest neighbors on the lattice.

Our model contains three parameters; λ_1 , λ_2 and λ_3 (Eq. 1). It is desirable that when executing the model it is reasonably robust with respect to these parameters. This will turn out to be the case in Sec. III when exploring the method.

As indicated in Sec. I, the above binary model shares similarities with the “diamond” encoding proposed in Ref. [16]. The latter method is able to reduce the number of binary variables required for very short chains, by fixing the position of the first bead and using the fact that odd and even beads can be assumed to belong to different “diamond” layers. For long chains, our choice of a freely moving chain on a simple odd/even checkerboard is more resource-efficient, because, in general, the search for the ground state can be carried out on a smaller grid if the chain is freely moving. Our constraint energies E_i also differ from those of Ref. [16]. In our case, all three constraint energies are manifestly non-negative for both physical and unphysical spin configurations, which makes our method more robust to changes in the strength parameters λ_i . Since the encoding in Ref. [16] was never explored, a robustness analysis is not available.

C. Simulated annealing

Before turning to QA, we tested this QUBO model using SA, with the system defined by the partition function $Z = \sum_{\{\sigma_s^f, \sigma_{s'}^{f'}\}} e^{-\beta E}$, where β denotes inverse temperature and E is given by Eq. 1. All runs spanned the same set of 25 temperatures, given by $\beta_0 = 1$ and $\beta_{i+1} = 1.05\beta_i$. At each temperature, 10^4 sweeps were performed, where one sweep comprises, on average, one attempted update per spin variable. The updates were single-spin flips, controlled by a Metropolis acceptance criterion. All runs were started from random initial spin configurations, and used a 10^2 grid.

For comparison, we also conducted SA runs based on the conventional explicit-chain representation of the HP model. Here, the energy was given by E_{HP} , without the constraint terms. The set of temperatures was the same as in the QUBO SA runs. The simulations used three Metropolis-type elementary moves: local one- and two-bead updates, and a non-local pivot update. At each temperature, 10^5 sweeps were performed, with one sweep consisting of $N - 1$ one-bead moves, $N - 2$ two-bead moves and one pivot move. The chains were not confined to a finite-size grid.

The QUBO SA simulations were run on a standard desktop computer. For $N = 30$, each

QUBO SA run required 21 CPU-core-seconds, whereas each explicit-chain SA run required 5 CPU-core-seconds. To gather statistics, for each sequence, we performed 1000 runs with each method, using different random number seeds.

D. Hybrid quantum-classical computations

D-Wave offers access to solvers based solely on QA as well as hybrid quantum-classical solvers. The hybrid approach uses classical solvers while sending suitable subproblems as queries to the quantum processing unit (QPU). The solutions to the subproblems serve to guide the classical solvers [22]. The goal is to speed up the solution of challenging QUBO problems by queries to the QPU. With the hybrid approach, it is possible to tackle much larger problems, with many thousands of fully connected variables, than what can be dealt with using QA alone.

We conducted hybrid quantum-classical computations for HP chains with up to 64 beads, using D-Wave’s hybrid solver services using a D-Wave Advantage quantum computer. All sequences were folded on a 10^2 grid. For $N = 64$ ($N = 30$), each hybrid run required 8 (4) seconds. To gather statistics, we performed 200 runs for the 64-bead sequence, and 100 runs for each of the other sequences.

E. Pure QPU computations

The 5000-qubit Advantage machine uses a Pegasus topology with a connectivity of 15 [21]. Thus, in order to solve a problem with higher connectivity, it has to be embedded into the Pegasus graph. This embedding is done by forming “chains” of qubits that act as single qubits. The strength of the coupling between the qubits within a chain is a tunable parameter, called the chain strength. This parameter is typically chosen slightly larger than the minimum chain strength needed to avoid chain breaks.

D-Wave offers several so-called samplers for finding embeddings into the QPU topology and performing the QPU computation. We used the `DWaveCliqueSampler`, designed for dense binary quadratic models. All the computations used a chain strength between 1 of 7.5 and the annealing time was set to $\tau = 2000 \mu\text{s}$, its maximum allowed value. The number of output reads per run, which must be $< 10^6/(\tau/\mu\text{s})$, was set to 490.

F. Testbed – HP sequences

As a testbed, we use a selected set of HP sequences with 14–30 beads, all of which are known from exhaustive enumerations to have a unique minimum-energy structure [18, 19]. The sequences are labeled S_N , where N indicates the number of beads, and are shown in Table A1.

A sequence having a unique minimum-energy structure is said to design that structure. The number of different sequences designing a given structure is called the designability of the structure. Structures with high designability thus show robustness to mutation.

For a given $N \leq 30$, in most cases, the selected sequence S_N is one of those that fold to the structure with highest designability for that N .

The sequences S_N can be found in Table A1, along with their minimum energies, E_{\min} . Some of the corresponding structures are shown in Fig. A1.

III. RESULTS

Using the spin representation of Sec. II B, we wish to find minimum-energy structures of given HP sequences by minimizing the total energy $E = E_{\text{HP}} + \sum_i \lambda_i E_i$ (Eq. 1) on a quantum annealer. As a first step toward this goal, we investigate the power of the QUBO approach under classical SA, and how it depends on the Lagrange parameters λ_i . We next do the same using the hybrid quantum-classical solver. Finally, we compare the results by using the QPU annealer only. We find that the hybrid quantum-classical solver outperforms all the other approaches listed above for our application.

A. Simulated annealing with QUBO encoding

In our binary model, the E_{HP} energy can become substantially lower than it is in any proper chain conformations. For this QUBO approach to work, it is therefore essential that the λ_i parameters that force the solutions to be “legal” are sufficiently large. On the other hand, by choosing large λ_i values, one risks making the energy landscape rugged, and therefore the dynamics potentially slow. Hence, the λ_i parameters should be neither too large nor too small.

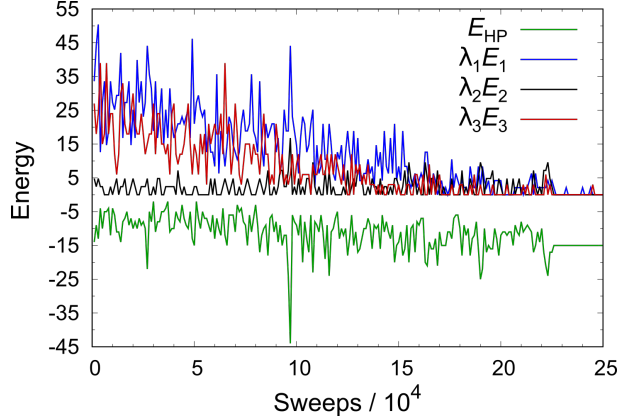


FIG. 2. Run-time evolution of the HP energy E_{HP} and the constraint energies E_1 , E_2 and E_3 in a QUBO SA folding simulation for the 30-bead sequence S_{30} (Table A1) on 10^2 grid, with $\lambda = (2.1, 2.4, 3.0)$.

To gain insight into the behavior of the binary model and its dependence on the λ_i parameters, we conducted a set of classical Monte Carlo-based SA runs (Sec. IIC), using the HP sequences S_{18} – S_{30} in Table A1. The runs had a fixed length and were deemed successful if the final state corresponded to the known minimum-energy structure of the given HP sequence. As expected, in order to have an acceptable hit rate, it was necessary to choose the λ_i parameters with some care. Nevertheless, without excessive fine-tuning, it was possible to find a single set of parameters, $\lambda = (2.1, 2.4, 3.0)$, that gave a hit rate $\gtrsim 0.1$ for all the sequences S_{18} – S_{30} (see below). We refrained from attempting any further optimization of the parameters, as the optimal values need not be the same on a quantum annealer. The optimal parameters would, of course, also depend on both HP sequence and grid size.

Figure 2 shows the run-time evolution of the four different energy terms in one of 1000 QUBO SA runs for the sequence S_{30} . At the end of the run, all the three constraint energies E_i vanish, while E_{HP} takes its known minimum value for an HP chain with this sequence ($E_{\text{min}} = -15$). Hence, the final spin configuration corresponds to the S_{30} ground state in the HP model. The hit rate, defined as the fraction of runs ending in the ground state, was 0.226 ± 0.013 . The remaining runs ended in spin configurations that either did not correspond to a proper chain, or corresponded to a structure with $E_{\text{HP}} > E_{\text{min}}$. In the beginning of the runs, the spin system undergoes a rapid relaxation, which brings the energies from initial values $E_{\text{HP}} \sim -10^3$ and $\lambda_1 E_1 + \lambda_2 E_2 + \lambda_3 E_3 \sim 10^5$ to the plotted range before the first

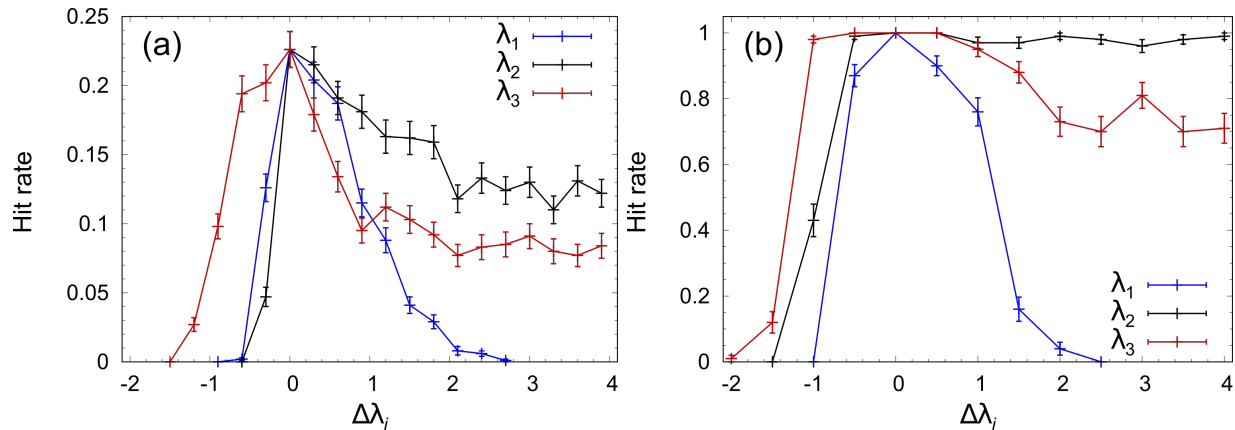


FIG. 3. Parameter dependence of the fraction of correct solutions (hit rate) in the vicinity of a reference point λ^* , when using QUBO SA and hybrid quantum-classical computation to search for the ground state of the S_{30} sequence (Table A1) on a 10^2 grid. The hit rate is plotted against $\Delta\lambda_i = \lambda_i - \lambda_i^*$, keeping $\lambda_j = \lambda_j^*$ for $j \neq i$. Lines are drawn to guide the eye. (A) QUBO SA with $\lambda = (2.1, 2.4, 3.0)$. (B) Hybrid quantum-classical computations with $\lambda = (2.0, 3.0, 3.0)$. Note the difference in scale between the two panels, reflecting the difference in performance as shown in Fig. 4.

measurement is taken (after 10^3 sweeps). We note that among the three constraint energies, E_1 and E_3 tend to relax much more slowly than E_2 , as is the case in Fig. 2. Note also that the HP energy takes values $E_{\text{HP}} < E_{\text{min}}$ many times during the course of the run. Such values can occur only when at least one constraint is broken.

Based on a limited set of preliminary runs, we chose $\lambda = \lambda^* = (2.1, 2.4, 3.0)$ for this QUBO SA run (Fig. 2). Figure 3(a) shows the parameter dependence of the hit rate in the vicinity of λ^* , when changing one λ_i at a time. In all three parameters, the hit rate stays tiny until a threshold is passed, followed by a step increase to the maximum observed hit rate, for $\lambda_i = \lambda_i^*$. When further increasing λ_i beyond λ_i^* , the hit rate decays, probably due to an increasingly rugged energy landscape. This decay leads to an upper limit on the parameter λ_1 , beyond which the hit rate is impractically small. By contrast, the hit rate stays significant even for λ_2 and λ_3 values much larger than those in Fig. 3(a). In fact, setting $\lambda_2 = 100$ or $\lambda_3 = 100$, we still obtained hit rates of 0.132 ± 0.011 and 0.074 ± 0.008 , respectively. Hence, overall the parameter sensitivity is low, although λ_1 must be chosen with some care.

The fact that the λ_1 dependence has a different shape than the dependencies on λ_2 and λ_3 can be, at least in part, understood. With the single-spin updates employed, the system cannot move from one chain-like configuration to another, both with $E_1 = E_2 = E_3 = 0$, without visiting intermediate non-chain configurations with $E_1 > 0$. By contrast, E_2 and E_3 may stay zero during such a move. This observation suggests that the energy landscape becomes rugged for large λ_1 , but not necessarily so for large λ_2 or λ_3 .

To explore how the performance of the QUBO SA approach depends on chain length, we conducted calculations for all the HP sequences S_{18} – S_{30} in Table A1, using $\boldsymbol{\lambda} = \boldsymbol{\lambda}^*$. As expected, the measured hit rates show a decreasing trend with increasing N (Fig. 4). However, the decrease is not monotonous, indicating that the hit rate is sequence-dependent and not a simple function of N .

For comparison, we also carried out a set of direct SA minimizations of E_{HP} based on conventional explicit-chain Monte Carlo methods (Fig. 4). Despite being faster, the hit rate is higher in these run than it is with QUBO-based SA. However, the difference in hit rate is modest given that state space for explicit chains is tiny is comparatively tiny. Note the similarities in shape between the hit rates obtained from these two unrelated sets of SA calculations. These similarities suggest that some target structures are relatively easy or difficult to find, independent of the method employed.

B. Hybrid quantum-classical computations

A promising alternative to pure QA is provided by hybrid quantum-classical methods, by which larger systems can be studied. To assess the power of this approach, we conducted hybrid computations for all the HP sequences studied in Sec. III A, S_{18} – S_{30} (Table A1). We additionally included a two longer sequences [20], which have been extensively used as testbeds for various (classical) methods.

As in the SA case, with the hybrid solver, a rough search was sufficient in order to find a single $\boldsymbol{\lambda}$, $\boldsymbol{\lambda}^* = (2.0, 3.0, 3.0)$, for which all the sequences S_{18} – S_{30} could be correctly folded on a 10^2 grid. Figure 3(b) shows the parameter dependence of the hit rate near $\boldsymbol{\lambda}^*$ when using the hybrid solver. Compared to QUBO SA (Fig. 3(a)), the measured hit rates are markedly higher with the hybrid solver (Fig. 4). At the same time, the λ_i dependencies share a similar shape in both cases. In particular, in both cases, the hit rate is more sensitive to changes

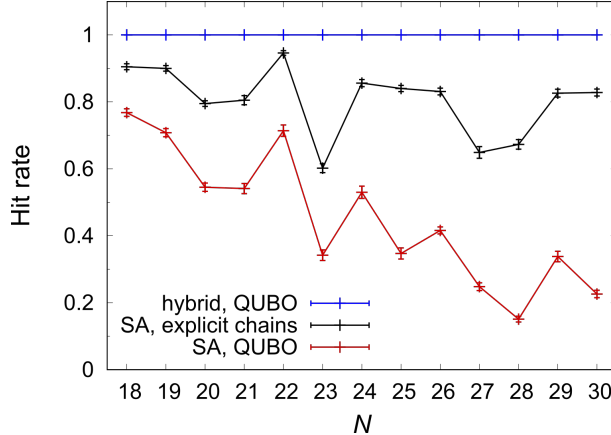


FIG. 4. Fraction of correct solutions (hit rate) when searching for the ground state of HP chains with $18 \leq N \leq 30$ beads by using the D-Wave hybrid solver with QUBO encoding (blue), SA with explicit chains (black) and SA with QUBO encoding (red). The HP sequences studied can be found in Table A1. The parameters λ were set to $(2.1, 2.4, 3.0)$ in the QUBO SA runs, and to $(2.0, 3.0, 3.0)$ when using the hybrid solver. All QUBO-based results were obtained using a 10^2 grid.

in λ_1 than to changes in λ_2 or λ_3 . As in the SA case, λ_2 or λ_3 can be chosen far above the plotted range in Fig. 3, without any major loss in hit rate. In fact, when setting $\lambda_2 = 100$ or $\lambda_3 = 100$, we obtained hit rates of 0.980 ± 0.014 and 0.54 ± 0.05 , respectively. Overall, the parameter sensitivity is lower with the hybrid solver than with QUBO SA.

When comparing hit rates from our hybrid and QUBO SA runs for the sequences S_{18} – S_{30} , we find that it is consistently highest in the hybrid case (Fig. 4). In fact, the hit rate is one across this entire set of sequences for the hybrid solver.

It is important to note that when folding the sequences S_{18} – S_{30} , the hybrid solver did not always make use of the QPU. The fraction of runs that used the QPU increased with N and was above one half for $N > 21$. Still, the precise contribution of the QPU to the final results is hard to judge since the details of the hybrid solver are not publicly available information. Nevertheless, the impressive results obtained for these sequences motivated us to also test the hybrid solver on two significantly longer sequences, namely S_{48} and S_{64} (Table A1) with 48 and 64 beads, respectively.

For these two sequences exact results are not available, but both belong to a set of HP sequences that have been widely used to test novel (classical) algorithms [20]. The lowest

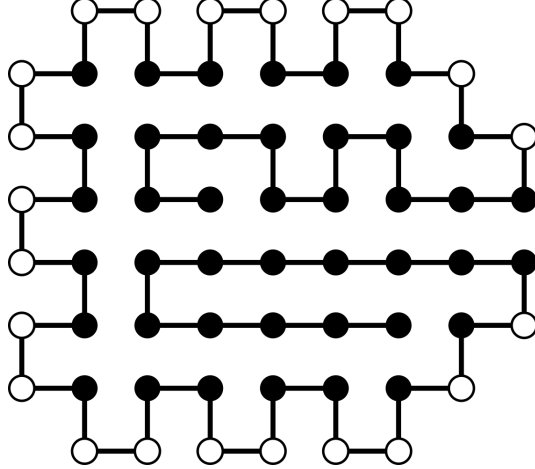


FIG. 5. The minimum-energy structure from hybrid classical-quantum computations for the 64-bead sequence S_{64} (Table A1), obtained using a 10^2 grid and $\lambda = (3.0, 4.0, 4.0)$. Filled and open symbols indicate H and P beads, respectively. The energy is $E_{HP} = -42$, which is the lowest known energy for this sequence [24].

known energies are $E_{HP} = -23$ for S_{48} [23] and $E_{HP} = -42$ for S_{64} [24]. We performed hybrid computations for both sequences on a 10^2 grid. In order to obtain good results, the λ_i parameters had to be adjusted. For S_{48} , the lowest known energy, $E_{HP} = -23$, was recovered in 10 of 100 hybrid runs, using $\lambda = (2.0, 3.5, 3.0)$. For S_{64} , with $\lambda = (3.0, 4.0, 4.0)$, a structure with the lowest known energy, $E_{HP} = -42$, was obtained in 1 of 200 hybrid runs. This folded structure is depicted in Fig. 5. Although the hit rate is low, it is encouraging that the hybrid solver is able to locate this complex low-energy structure.

C. Pure QPU computations

The QUBO problem that we wish to solve for finding minimum-energy HP structures contains $\approx NL^2/2$ logical qubits. Moreover, the system is almost fully connected, implying that its embedding into the QPU topology requires a significant amount of additional qubits. Therefore, pure QPU computation is effectively limited to relatively short HP chains.

To explore how the performance of the pure QPU approach depends on system size, we conducted computations for the six sequences S_4 , S_6 , S_7 , S_8 , S_9 and S_{10} (Table A1) for various grid sizes. Figure 6(a) shows the fraction of all annealing cycles that recovered the known minimum-energy structure, for these systems, plotted against the number of physical

qubits employed. The parameters λ_i and the annealing time were the same for all systems, whereas the chain strength was chosen individually for each system, for best performance (among the values 1.0, 1.5, ..., 4.5, 5.0). Albeit with some scatter, the hit rate shows a roughly exponential decay with system size. This system-size dependence is more severe than the above-mentioned scaling of the number of qubits required, and remedies are being explored [25].

The longest sequence that was successfully folded in our pure QPU computations was S_{14} with 14 beads (Table A1). This sequence, whose minimum-energy structure can be seen in Fig. 6(b), was studied using a 4^2 grid, which required 112 logical and 1214 physical qubits. The chain strength was set to 7.5. To our knowledge, this is the largest protein successfully folded using a quantum computer. However, the ground state was only recovered in one of a total of 100×490 annealing cycles. This number of cycles is larger than the number of distinct conformations available to a chain with 14 beads on a 4^2 grid, which is 416. On the other hand, it is tiny compared to the $2^{112} \approx 5.2 \times 10^{33}$ states of the binary system, the vast majority of which do not correspond to proper chain configurations. Finally, we note that our S_{14} system is similar in size to the largest system solved in a recent benchmarking study of the D-Wave Advantage machine using exact cover problems, which contained 120 logical qubits [26].

It is possible that the pure QPU results can be improved by further tuning of the simulation parameters. However, at present, we conclude that pure QPU computation cannot match classical SA or the hybrid quantum-classical approach (Secs. III A, III B).

IV. SUMMARY AND OUTLOOK

We have developed a novel mapping of the two-dimensional HP lattice protein model onto a quantum annealer, which is successfully explored on the D-Wave Advantage system. This simplified model for protein structures is known to represent a quite difficult optimization problem when determining structure using conventional classical methods. As benchmarks for success, we used HP chains with sizes ranging from $N = 4$ to $N = 30$, for which the exact solutions are known from exhaustive enumerations. For larger problems, with $N = 48$ and $N = 64$, we compared with the best known solutions obtained by classical means. The approach allows us to explore the largest chains studied so far on a quantum annealer, and

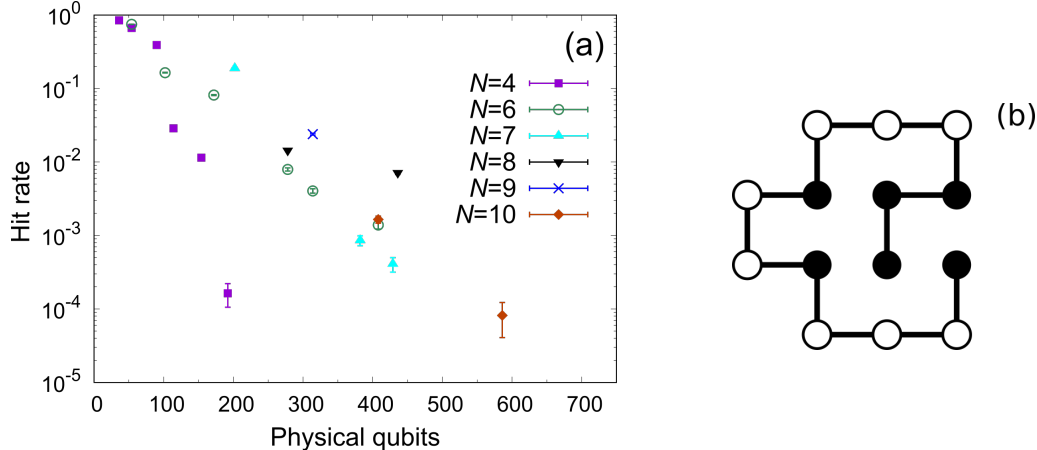


FIG. 6. Pure QPU computations. For every choice of sequence and grid size studied, we conducted 100 runs with 490 annealing cycles each. The sequences can be found in Table A1. (A) The hit rate on a logarithmic scale against the number of physical qubits used for the sequences S_4 , S_6 , S_7 , S_8 , S_9 and S_{10} for various grid sizes, using $\lambda = (1.0, 2.0, 1.5)$. Statistical errors are comparable with or smaller than the symbol sizes. (B) The minimum-energy structure for the sequence S_{14} , which was successfully recovered on a 4^2 grid, using $\lambda = (2.0, 7.0, 4.0)$. Filled and open symbols indicate H and P beads, respectively.

consistently provides high percentages of correct solution on multiple runs. However, the success of our approach relies upon using the hybrid variant provided by D-Wave. The performance of pure QA is less impressive with a drastic decrease in success rate as the system size is increased. These calculations were therefore limited to chains with at most $N = 14$.

Our approach differs from previous attempts based upon growth algorithms, as it maps the problem onto a lattice spin system where the spins, or qubits, are present throughout the lattice. In comparison to earlier work, this representation greatly facilitates the handling of interactions, including self-avoidance. Furthermore, except for very short chains, this representation is more resource-efficient, as the amount of logical qubits required exhibits a polynomial rather than exponential scaling with chain length.

The encoding requires penalty terms for the global energy minimum of the spin system to correspond to a proper chain. The method is robust to changes in the strengths of the penalty terms, which require only a modest amount of tuning.

For convenience, we have focused on the HP model with its minimal two-letter alphabet.

To extend the approach to models with larger alphabets, such as the 20-letter Miyazawa-Jernigan model [27], is straightforward, as it amounts to simply changing the interaction parameters in Eq. 2. Moreover, although the checkerboard division into even and odd sites may have to be modified or abandoned, the method can be applied to an arbitrary graph. In particular, it can be directly applied to three-dimensional grids, including the tetrahedral one used in Ref. [13].

Finally, we note that a similar approach could be applicable to gate-based quantum computers. This could potentially take the form of a quantum variational algorithm or a quantum search algorithm.

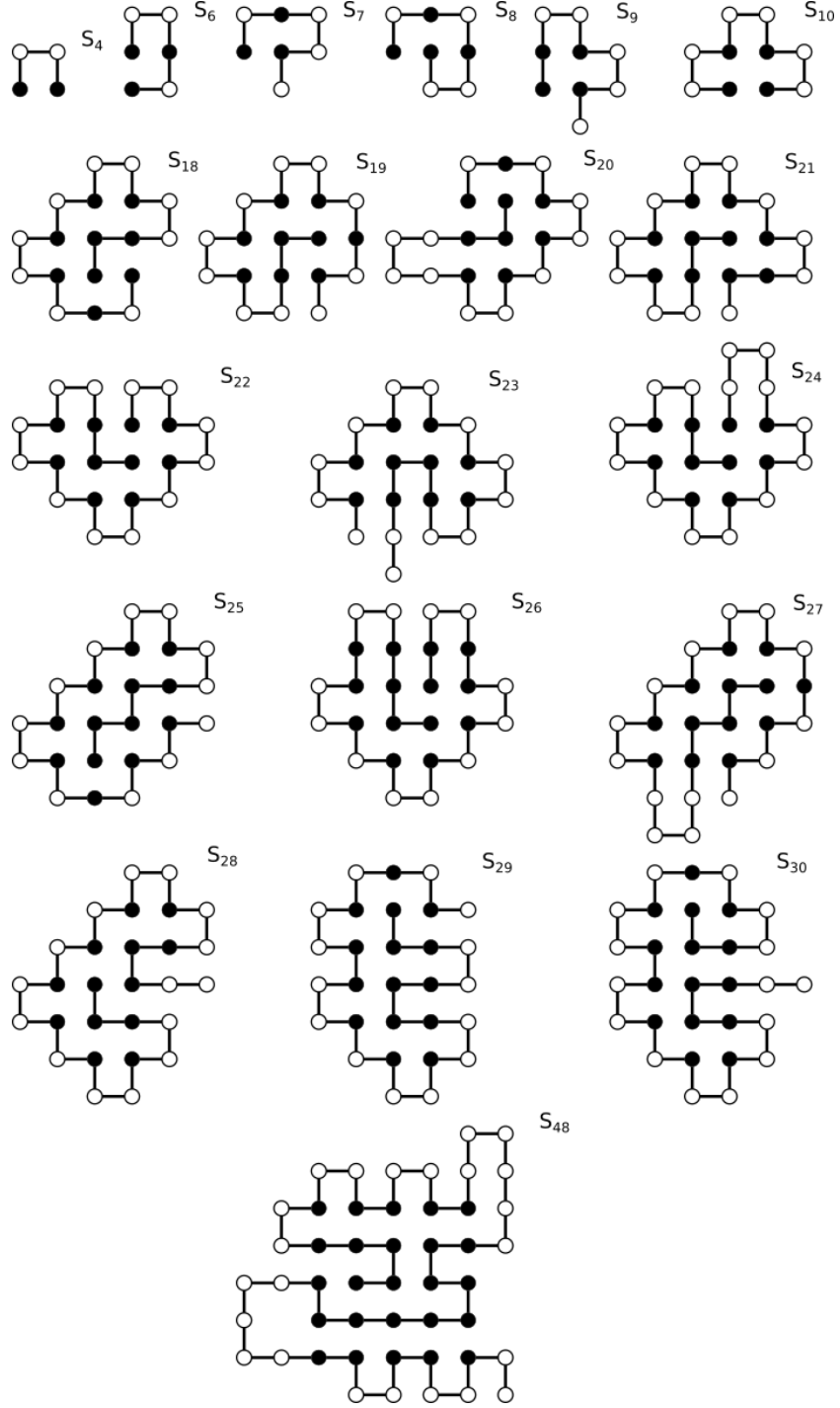


FIG. A1. Ground states for all the sequences S_N in Table A1 with $N \leq 30$ [18, 19] except S_{14} (whose ground state can be found in Fig. 6(b)). Also shown is an S_{48} structure, which is one of 10 structures with the lowest known energy ($E_{\text{HP}} = -23$) for this sequence found using the hybrid solver. A low-energy structure for the sequence S_{64} in Table A1 can be found in Fig. 5.

ACKNOWLEDGMENTS

This work was in part supported by the Swedish Research Council (Grant no. 621-2018-04976). We gratefully acknowledge the Jülich Supercomputing Centre (<https://www.fz-juelich.de/ias/jsc>) for supporting this project by providing computing time on the D-Wave Advantage™ System JUPSI through the Jülich UNified Infrastructure for Quantum computing (JUNIQ). We have enjoyed fruitful discussions with theory group members at the Wallenberg Centre for Quantum Technology at Chalmers University. In particular, we would like to thank Hanna Linn for feedback on the code.

-
- [1] M. W. Johnson, M. H. S. Amin, S. Gildert, T. Lanting, F. Hamze, N. Dickson, R. Harris, A. J. Berkley, J. Johansson, P. Bunyk, E. M. Chapple, C. Enderud, J. P. Hilton, K. Karimi, E. Ladizinsky, N. Ladizinsky, T. Oh, I. Perminov, C. Rich, M. C. Thom, E. Tolkacheva, C. J. S. Truncik, S. Uchaikin, J. Wang, B. Wilson, and G. Rose, Quantum annealing with manufactured spins, *Nature* **473**, 194 (2011).
- [2] F. Arute, K. Arya, R. Babbush, D. Bacon, J. C. Bardin, R. Barends, R. Biswas, S. Boixo, F. G. S. L. Brandao, D. A. Buell, B. Burkett, Y. Chen, Z. Chen, B. Chiaro, R. Collins, W. Courtney, A. Dunsworth, E. Farhi, B. Foxen, A. Fowler, C. Gidney, M. Giustina, R. Graff, K. Guerin, S. Habegger, M. P. Harrigan, M. J. Hartmann, A. Ho, M. Hoffmann, T. Huang, T. S. Humble, S. V. Isakov, E. Jeffrey, Z. Jiang, D. Kafri, K. Kechedzhi, J. Kelly, P. V. Klimov, S. Knysh, A. Korotkov, F. Kostritsa, D. Landhuis, M. Lindmark, E. Lucero, D. Lyakh, S. Mandrà, J. R. McClean, M. McEwen, A. Megrant, X. Mi, K. Michielsen, M. Mohseni, J. Mutus, O. Naaman, M. Neeley, C. Neill, M. Y. Niu, E. Ostby, A. Petukhov, J. C. Platt, C. Quintana, E. G. Rieffel, P. Roushan, N. C. Rubin, D. Sank, K. J. Satzinger, V. Smelyanskiy, K. J. Sung, M. D. Trevithick, A. Vainsencher, B. Villalonga, T. White, Z. J. Yao, P. Yeh, A. Zalcman, H. Neven, and J. M. Martinis, Quantum supremacy using a programmable superconducting processor, *Nature* **574**, 505 (2019).
- [3] T. Kadowaki and H. Nishimori, Quantum annealing in the transverse Ising model, *Phys. Rev. E* **58**, 5355 (1998).
- [4] J. Brooke, D. Bitko, T. F. Rosenbaum, and G. Aeppli, Quantum annealing of a disordered

- magnet, *Science* **284**, 779 (1999).
- [5] S. Boixo, T. F. Rønnow, S. V. Isakov, Z. Wang, D. Wecker, D. A. Lidar, J. M. Martinis, and M. Troyer, Evidence for quantum annealing with more than one hundred qubits, *Nat. Phys.* **10**, 218 (2014).
 - [6] S. Kirkpatrick, C. D. Gelatt, and M. P. Vecchi, Optimization by simulated annealing, *Science* **220**, 671 (1983).
 - [7] J. J. Hopfield and D. W. Tank, Neural computation of decisions in optimization problems, *Biol. Cybern.* **52**, 141 (1985).
 - [8] C. Peterson and J. R. Anderson, Neural networks and NP-complete problems; a performance study of the graph bisectioning problem, *Complex Syst.* **2**, 59 (1988).
 - [9] A. Lucas, Ising formulations of many NP problems, *Front. Phys.* **2**, 1 (2014).
 - [10] A. Perdomo, C. Truncik, I. Tubert-Brohman, G. Rose, and A. Aspuru-Guzik, Construction of model hamiltonians for adiabatic quantum computation and its application to finding low-energy conformations of lattice protein models, *Phys. Rev. A* **78**, 012320 (2008).
 - [11] K. F. Lau and K. A. Dill, A lattice statistical mechanics model of the conformational and sequence spaces of proteins, *Macromolecules* **22**, 3986 (1989).
 - [12] A. Perdomo-Ortiz, N. Dickson, M. Drew-Brook, G. Rose, and A. Aspuru-Guzik, Finding low-energy conformations of lattice protein models by quantum annealing, *Sci. Rep.* **2**, 248 (2012).
 - [13] A. Robert, P. K. Barkoutsos, S. Woerner, and I. Tavernelli, Resource-efficient quantum algorithm for protein folding, *Npj Quantum Inf.* **7**, 38 (2021).
 - [14] C. Outeiral, G. M. Morris, J. Shi, M. Strahm, S. C. Benjamin, and C. M. Deane, Investigating the potential for a limited quantum speedup on protein lattice problems, *New J. Phys.* **23**, 103030 (2021).
 - [15] C. Micheletti, P. Hauke, and P. Faccioli, Polymer physics by quantum computing, *Phys. Rev. Lett.* **127**, 080501 (2021).
 - [16] R. Babbush, A. Perdomo-Ortiz, B. O’Gorman, W. Macready, and A. Aspuru-Guzik, Construction of energy functions for lattice heteropolymer models: efficient encodings for constraint satisfaction programming and quantum annealing, *Adv. Chem. Phys.* **155**, 201 (2014).
 - [17] B. A. Reva and A. V. Finkelstein, Search for the most stable folds of protein chains: II. Computation of stable architectures of β -proteins using a self-consistent molecular field theory, *Protein Eng. Des. Sel.* **9**, 399 (2014).

- [18] A. Irbäck and C. Troein, Enumerating designing sequences in the HP model, *J. Biol. Phys.* **28**, 1 (2002).
- [19] C. Holzgräfe, A. Irbäck, and C. Troein, Mutation-induced fold switching among lattice proteins, *J. Chem. Phys.* **135**, 195101 (2011).
- [20] R. Unger and J. Moult, Genetic algorithms for protein folding simulations, *J. Mol. Biol.* **231**, 75 (1993).
- [21] C. McGeoch and P. Farré, *The D-Wave Advantage System: an overview*, Tech. Rep. (D-Wave Systems Inc., 2020).
- [22] C. McGeoch, P. Farré, and W. Bernoudy, *D-Wave Hybrid Solver Service + Advantage: technology update*, Tech. Rep. (D-Wave Systems Inc., 2020).
- [23] F. Liang and W. H. Wong, Evolutionary Monte Carlo for protein folding simulations, *J. Chem. Phys.* **115**, 3374 (2001).
- [24] U. Bastolla, H. Frauenkron, E. Gerstner, P. Grassberger, and W. Nadler, Testing a new Monte Carlo algorithm for protein folding, *Protein Eng.* **32**, 52 (1998).
- [25] A. Pearson, A. Mishra, I. Hen, and D. A. Lidar, Analog errors in quantum annealing: doom and hope, *Npj Quantum Inf.* **5**, 107 (2019).
- [26] D. Willsch, M. Willsch, C. D. G. Calaza, F. Jin, H. De Raedt, M. Svensson, and K. Michielsen, Benchmarking Advantage and D-Wave 2000Q quantum annealers with exact cover problems, *Quantum Inf. Process.* **21**, 141 (2022).
- [27] S. Miyazawa and R. L. Jernigan, Residue-residue potentials with a favorable contact pair term and an unfavorable high packing density term, for simulation and threading, *J. Mol. Biol.* **256**, 623 (1996).